Effect of channel temperature and mass window in the fission decay of ^{181}Re*

C. Kokila and M. Balasubramaniam*
Department of Physics, Bharathiar University, Coimbatore 641046, India

(Received 10 September 2019; revised manuscript received 19 November 2019; published 22 January 2020)

The dynamical cluster-decay model (DCM) with mass window restriction and channel temperature is applied to study the decay of hot and rotating compound nucleus ^{181}Re* formed through the reaction ^{12}C + ^{169}Tm at three different experimental incident energies, 77.18, 83.22, and 89.25 MeV, for spherical and deformed fragments. So far in DCM, the evaluation of various fission observables such as mass and charge distribution, decay cross section, kinetic energy, excitation energy, etc., were studied considering the entire mass range covering the limiting values of the mass asymmetry from 0 to 1, accounting for emission of light particles, complex intermediate mass fragments, as well as fission fragments. These emissions are considered as the dynamical collective mass motion of preformed clusters through the barrier. In this work, restriction of the mass window is considered in DCM as that of the experimental data for which cross section of the fission fragments is measured. The mass window restriction enhances the formation probability of the fragments. Further, instead of using a fixed temperature for all mass asymmetries (or channels), temperature tuning is attempted to see its effect on the outcome of the model. The obtained results of cross section values are found to compare reasonably well with the experimental data.

DOI: 10.1103/PhysRevC.101.014614

I. INTRODUCTION

In low energy heavy-ion collisions, apart from light particle emission ($A \leqslant 4$), intermediate mass fragment (fission fragment) emission has been investigated in light to medium mass parent nuclei. Though the emission of light particles can happen either through direct reaction or from preequilibrium emission, the fission fragment emission along with light particle emission usually takes place from an equilibrated compound nucleus, which is mainly dictated by the excitation energy imparted to it. In such fusion-fission reactions, there is always a competition between light particle emission and fission fragment emission. Conventionally, the light particle emission is always treated within the statistical picture, and fission type models such as the scission point model or the saddle point fission model are used to account for the emission and dynamics of fission fragments.

Different theoretical models explain the binary decay of the compound nucleus in the light and the heavy mass regions. Light heavy-ion fusion reactions are explained using the extended Hauser-Feshbach method (EHFM) [1]. This formalism assumes the fission probability to be proportional to the available phase space at the scission point. In this method, the cross section of the compound nucleus formation at a certain excitation energy and angular momentum is proportional to the decay ratio, which is determined by the ratio of partial width to the total width. The partial width is related to phase-space integration, which in turn depends on the level density of the compound state. For the calculation of evaporation residues, statistical-model codes like CASCADE, PACE, or LILITA use the Hauser-Feshbach formalism. The saddle point model [2,3] requires knowledge of the macroscopic fission barrier as functions of the spin and mass asymmetries of the decaying channels. Saddle points were located using suitable shape parametrization, and the saddle point energies calculated depend on Coulomb, rotational, and nuclear energies. This model accounts for the fusion cross section of the compound nucleus in the light mass region and depends on its spin distribution. The fission width is calculated using the level density, which is evaluated using the Fermi-gas formula. The scission point model [4,5] relies on the assumption that the properties of the fission fragment distributions depend on the available energy of the different configurations at the scission point. Fission fragments are assumed to be deformed and are separated. Wilkins *et al.* used an exponential dependence on the potential to evaluate the mass distribution, whereas Lemaître *et al.* used a level density calculation to determine fragmentation yield.

However, the dynamical cluster-decay model (DCM) of Gupta and collaborators [6–8] takes into account both the light particle emission and fission fragment emission at the same level of theory based on the quantum mechanical fragmentation process. The uniqueness of this model is that, to account for the structure effects, the DCM considers the fragment (or cluster) preformation in the compound nucleus before the fragments undergo subsequent decay as in a cluster decay process. Within DCM, temperature effects [7,9–11] and deformation and orientation effects [12] were included to calculate the actual cross sections and average kinetic energies of the light particles and heavy fragments. Since the compound nucleus has the excitation energy from the entrance channel, the temperature (T) dependence in the model is important to account for the cross section and kinetic energy values from

*m.balou@gmail.com

the experimental results. In Ref. [13], a reformulated DCM which uses Krappe's T-dependent binding energy formula [14] is reported.

Thus far, in DCM, in the calculation of fragments cross section of fission fragments emitted from the compound nucleus (CN) formed in low energy heavy ion induced reactions, the complete mass window has been taken into account. It may be appropriate to study the effect of restriction of the mass window if the parent nucleus mass is heavy. The mass window region can be chosen either based on experimental observation or by studying its role for different mass windows. Such mass window restriction was recently reported by us [15] for the neutron-induced fission of ^{235}U within fragmentation theory. Further, in DCM, for the deexcitation studies of compound nuclei formed in heavy-ion reactions, the temperature for the fragmentation process is considered to correspond to the excitation energy of the compound nucleus (E^*_{CN}). However, at the instant of scission (at fixed distance R, defined later), the available excitation energy of the compound nucleus E^*_{CN} has to be distributed to the two subsystems. In this scenario, the temperature corresponding to the compound nucleus may not conserve the total energy of the two subsystems, demanding the tuning of temperature for each channel. This available excitation energy at scission will then be liberated as the kinetic energy, excitation energy, and Q value of the fragments. A deexcitation study discussing the effect of channel temperature over a constant temperature within the statistical theory and level density approach was reported recently [16] for the calculation of ternary fragmentation potential energies of ^{252}Cf. Also, in another recent work [17], the mass distribution of neutron-induced binary and ternary fission of ^{235}U within a modified scission point model considered the effect of channel temperature. Recently, in Ref. [15], a detailed account of channel temperature in the calculation of the mass distribution of neutron-induced fission of ^{235}U was reported. The present work is a sequel to our earlier reported work on neutron-induced fission [15]. In this work, the role of deformation of the fragments is also considered.

In this work, our interest is to see the effect of channel temperature and choice of the mass window on the deexcitation of the compound nucleus formed in heavy-ion induced reactions within DCM. For our study, we have considered a recent work of Sood *et al.* [18], in which the fission fragment cross sections of the compound nucleus ^{181}Re* formed through the reaction ^{12}C + ^{169}Tm at three different laboratory energies, $E_{\rm lab}$ = 77.18, 83.22, and 89.25 MeV, are reported. There has been experimental interest in the production of proton-rich isotopes of Re (a higher homologue of technetium and with a more favorable half-life than technetium) as it may find clinical applications as an alternative to ^{99m}Tc (see [19] and references therein). Several experimental investigations were carried out using light ion induced reactions for the production of proton-rich to neutron-rich Re isotopes. The heavy-ion induced reactions are also of interest for the production of Re isotopes. In one such study Lahiri *et al.* [20] reported the production of ^{181}Re through ^{16}O activation on a natural thulium target. The complete as well as the incomplete fusion of the reaction ^{12}C + ^{169}Tm were studied by Chakrabarty *et al.* in [21]. They measured the cross section of evaporation residues in the ^{12}C + ^{169}Tm reaction over a range of beam energies from 60 to 84 MeV. They studied the competition of complete and incomplete fusion processes by studying the recoil-range distributions using the recoil-catcher technique and offline γ-ray spectrometry. Further, the ^{181}Re* compound system formed through ^{16}O + ^{165}Ho and ^{12}C + ^{169}Tm have also been reported in Refs. [22,23]. Using a stacked foil activation technique with incident energies near the Coulomb barrier, Sharma *et al.* [23] reported the preequilibrium emission process of the fusion reactions of ^{12}C with ^{128}Te and ^{169}Tm, and of ^{16}O with ^{159}Tb and ^{169}Tm. They calculated the cross sections of the evaporation residues as a function of energy, which was compared with the results from the statistical code PACE4 [24]. Such radionuclides with characteristic activity, half-life, and decay mode may be useful for medical applications.

In the experiment of Ref. [18], the reaction products were identified based on their characteristic γ rays and half-lives obtained from the decay curve analysis. The intensities of the observed γ rays were then used to calculate the formation cross section of evaporation residues. Using the recoil-catcher activation technique followed by offline γ spectroscopy, the production cross sections for fission-like events were measured. Twenty-six fission-like events with fragment charge numbers between 32 and 49 were identified, corresponding to three different excitation energies of 57, 63, and 69 MeV. They observed a broad and symmetric mass distribution of the fission fragments, emphasizing their production via the compound nuclear process. The mass window range from mass numbers 75 to 106 corresponding to the experimental fission-like events is considered in the present study. The selection of mass window restriction is simply based on the reported experimental mass window.

The details of the dynamical cluster model will be described briefly in the following section. In the subsequent sections, the results and summary are presented.

II. METHOD

Gupta and collaborators developed the dynamical cluster-decay model for hot and rotating nuclei based on the preformed cluster model (PCM) [25,26] for ground-state decays. In DCM, the complex fragments (the intermediate mass fragments or clusters) and light particles are treated as the dynamical collective mass motion of preformed fragments through the barrier. The dynamical collective clusterization process is referred to as a possible alternative of the fission process. In terms of the barrier picture, a cluster-decay process is a fission process with structure effects of the CN included through the preformation of the fragments, but without any phase-space arguments. The PCM and DCM find their roots in the quantum mechanical fragmentation theory (QMFT) [26–28], developed for fission and heavy-ion reactions and used later for predicting exotic cluster radioactivity. Further, the dynamical fragmentation theory is based on the asymmetric two-center shell model (ATCSM) [29]. The two-center shell model provides the microscopic part of the potential energy surface. QMFT is a unified description of both fission

(including cluster radioactivity) and fusion (heavy-ion collisions) of nuclei. This theory uses a set of coordinates to characterize the nuclear shape evolved during fission. This theory works in terms of the collective coordinates of the mass and charge asymmetries, defined as

$$\eta = (A_1 - A_2)/(A_1 + A_2)$$

and

$$\eta_Z = (Z_1 - Z_2)/(Z_1 + Z_2),$$

where A_i and Z_i $(i = 1, 2)$ are the mass and charge numbers, with 1 and 2 referring to heavy and light fragments respectively. The other coordinate of this model is the relative separation R between the fragments.

For the reaction under study, viz., $^{12}\mathrm{C} + {}^{169}\mathrm{Tm} \rightarrow {}^{181}\mathrm{Re}^*$, the entrance channel Q value, known as Q_{in}, is -14.768 MeV. This Q_{in} adds to the entrance channel kinetic energy $E_{\mathrm{c.m.}}$, giving the excitation energy of the compound nucleus E^*_{CN} as

$$E^*_{CN} = E_{\mathrm{c.m.}} + Q_{\mathrm{in}}. \tag{1}$$

It is assumed that the total excitation energy of the compound nucleus E^*_{CN} is distributed to binary subsystems at the saddle point as

$$E^*_{CN} = (E^*_1 + E^*_2)|_{\mathrm{saddle}}, \tag{2}$$

where the individual excitation energies of the two fragments at saddle are evaluated using $E^*_i = BE(T)_i - BE(T = 0)_i$ with $i = 1, 2$. Here $BE(T)_i$ and $BE(T = 0)$ are the temperature dependent binding energy at temperature T_i and at $T = 0$ respectively. To evaluate the temperature-dependent binding energy, Krappe's T-dependent binding energy formula is used [13]. In the exit channel, beyond the saddle point, the total excitation energy of the compound nucleus E^*_{CN} is contributed by the Q value of the outgoing channel, the total kinetic energy (TKE), and the total excitation energy (TXE) of the outgoing fission fragments as

$$E^*_{CN} = Q_{\mathrm{out}} + \mathrm{TKE} + \mathrm{TXE}. \tag{3}$$

In DCM, thus far, the temperature of all channels is taken to be constant, corresponding to the excitation energy of the compound nucleus, denoted as T_{CN} in MeV and is related to the excitation energy, E^*_{CN}, as

$$E^*_{CN} = (A/9)T^2_{CN} - T_{CN}. \tag{4}$$

Here, instead of a fixed temperature, the temperature for each channel, T_η, is iteratively obtained, such that Eq. (2) is satisfied. This temperature T_η is then used to determine the temperature-dependent fragmentation potential $V(\eta, T_\eta, \beta, \ell)$ at a fixed R and deformation [30], and is given by

$$\begin{aligned} &V(\eta, T_\eta, \beta, \ell) \\ &= -\sum_{i=1}^{2}[BE_{LDM}(A_i, Z_i, T_\eta)] + \sum_{i=1}^{2}\delta U_i(T_\eta)\exp\left(-\frac{T^2_\eta}{T^2_0}\right) \\ &\quad + E_C(\beta, T_\eta) + V_P(\beta, T_\eta) + V_\ell(\beta, T_\eta). \end{aligned} \tag{5}$$

The first term is evaluated using Krappe's binding energy formula. The shell corrections δU_i are taken to go to zero exponentially with T, with $T_0 = 1.5$ MeV [31]. The fragments are treated as deformed with deformation values taken from Möller's mass table [30]. Here only the quadrupole deformation is considered. The Coulomb potential for deformed fragments [32] is

$$E_C(\beta, T_\eta) = E_{C_0}\{1 + E_{C_1} + E_{C_2} + E_{C_3} + E_{C_4}\}, \tag{6}$$

with

$$\begin{aligned} E_{C_0} &= \frac{Z_1 Z_2 e^2}{R_t(T_\eta)}, \\ E_{C_1} &= \frac{3}{2\sqrt{5\pi}R_t{}^2(T_\eta)}\left[R^2_{01}(T_\eta)\beta_1 + R^2_{02}(T_\eta)\beta_2\right], \\ E_{C_2} &= \frac{3}{7\pi R^2_t(T_\eta)}\left[R^2_{01}(T_\eta)\beta^2_1 + R^2_{02}(T_\eta)\beta^2_2\right], \\ E_{C_3} &= \frac{9}{14\pi R^4_t(T_\eta)}\left[R^4_{01}(T_\eta)\beta^2_1 + R^4_{02}(T_\eta)\beta^2_2\right], \\ E_{C_4} &= \frac{27R^2_{01}(T_\eta)R^2_{02}(T_\eta)}{10\pi R^4_t(T_\eta)}\beta_1\beta_2. \end{aligned}$$

β_1 and β_2 are the quadrupole deformations of heavy and light fragments respectively. R_t is the distance between the centere of the deformed fragments corresponding to an orientation of $\theta = 0$, and the touching configuration is defined as $R_t = R_1 + R_2 + \Delta R$ with the radii of deformed nuclei

$$R_i(\theta_i) = R_{0i}[1 + \beta_i Y_{20}(\theta_i)]. \tag{7}$$

R_{0i} is the radii of spherical nuclei of mass number A_i $(i = 1, 2)$, which is evaluated as

$$R_{0i}(T_\eta) = \left[1.28A_i^{1/3} - 0.76 + 0.8A_i^{-1/3}\right]\left(1 + 0.0007T^2_\eta\right). \tag{8}$$

ΔR is the only free parameter of the model and is referred to as the neck-length parameter.

The nuclear potential is given by

$$V_P(\beta, T_\eta) \approx S(\beta_1, \beta_2)V_{N0}(T_\eta). \tag{9}$$

The strength of nuclear interaction introduced by deformation is included through the factor $S(\beta_1, \beta_2)$. V_{N0} is the nuclear part of the interaction potential between the same nuclei, but with spherical shapes. The smallest distances between the surfaces of spherical and deformed nuclei are taken to be same. The factor $S(\beta_1, \beta_2)$ is related to the surface curvatures of deformed nuclei [33] as

$$S(\beta_1, \beta_2) = \frac{\frac{R^2_1(\pi/2)R^2_2(\pi/2)}{R^2_1(\pi/2)R_2(0)+R^2_2(\pi/2)R_1(0)}}{\frac{R_{01}R_{02}}{R_{01}+R_{02}}}. \tag{10}$$

For the nuclear part of the interaction potential corresponding to spherical nuclei, the Blocki [34] prescription is used. The proximity potential for the spherical fragments is defined as

$$V_{N0}(T_\eta) = 4\pi\bar{R}\gamma b(T_\eta)\phi[s(T_\eta)], \tag{11}$$

where $\bar{R}$ is the inverse of the root-mean-square radius and is given by

$$\bar{R} = \frac{R_{01}R_{02}}{R_{01} + R_{02}}, \tag{12}$$

and $\phi[s(T_\eta)]$, the universal function, is given as

$$\phi[s(T_\eta)] = \begin{cases} -\frac{1}{2}\xi^2 - 0.0852\xi^3, & s \leqslant 1.251, \\ -3.437\exp\left(-\frac{s}{0.75}\right), & s \geqslant 1.251, \end{cases} \quad (13)$$

with $\xi = (s - 2.54)$, and γ, the nuclear surface energy term is given by

$$\gamma = 0.9517\left[1 - 1.7826\left(\frac{N-Z}{A}\right)^2\right]. \quad (14)$$

The overlap or separation distance, in units of b, between the two colliding surfaces is

$$s(T_\eta) = \frac{R_t^{sph} - (R_{01} + R_{02})}{b(T_\eta)}, \quad (15)$$

with surface width $b(T_\eta) = 0.68(1 + 7.37 \times 10^{-3} T_\eta^2)$, and R_t^{sph} is the relative separation corresponding to spherical nuclei at the touching point and is defined as $R_t^{sph} = R_{01} + R_{02} + \Delta R$.

Similarly, the centrifugal potential is defined as

$$V_\ell(\beta, T_\eta) = \frac{\hbar^2 \ell(\ell+1)}{2I_S(\beta, T_\eta)}, \quad (16)$$

where, in the complete sticking limit, the moment of inertia is

$$I_S(\beta, T_\eta) = \mu R_t^2(T_\eta) + \tfrac{2}{5}A_1 m R_1^2(T_\eta) + \tfrac{2}{5}A_2 m R_2^2(T_\eta), \quad (17)$$

with $\mu = \frac{A_1 A_2}{A_1 + A_2} m$ being the reduced mass and m being the nucleon mass.

Using the decoupled approximation to R and η motion, the preformation probability P_0 referring to η motion and penetration probability, P referring to R motion can be obtained. The preformation probability of the fragments is obtained by solving the stationary Schrödinger equation governing the η coordinate motion at a fixed $R = R_t$:

$$\left\{-\frac{\hbar^2}{2\sqrt{B_{\eta\eta}}}\frac{\partial}{\partial\eta}\frac{1}{\sqrt{B_{\eta\eta}}}\frac{\partial}{\partial\eta} + V_R(\eta, \beta, T_\eta)\right\}\psi^\nu(\eta) = E^\nu \psi^\nu(\eta), \quad (18)$$

with $\nu = 0, 1, 2, 3, \ldots$ corresponding respectively to the ground and excited states. The normalization then gives the preformation probability as

$$P_0(A_i) = |\psi[\eta(A_i)]|^2 \sqrt{B_{\eta\eta}}\frac{2}{A}, \quad (19)$$

A being the mass number of the compound nucleus and $i = 1, 2$. The kinetic energy part in Eq. (18) is represented using the hydrodynamical mass of Kröger and Scheid [35]. At temperature T, the preformation factor P_0 is calculated with temperature effects included in $\psi(\eta)$ through a Boltzmann-like function as

$$|\psi|^2 = \sum_{\nu=0}^{\infty} |\psi^\nu|^2 \exp(-E^\nu/T_{CN}). \quad (20)$$

The barrier penetration probability P is obtained using the Wentzel-Kramers-Brillouin approximation governing the R motion at a fixed η:

$$P = \exp\left[-\frac{2}{\hbar}\int_{R_a}^{R_b}\{2\mu[V_\eta(R, \beta, T_\eta) - Q_{\rm eff}]\}^{1/2} dR\right]. \quad (21)$$

R_a and R_b are the first and second turning point satisfying $V_\eta(R_a) = V_\eta(R_b) = Q_{\rm eff}$. The scattering potential $V_\eta(R, \beta, T_\eta)$ is defined as

$$V_\eta(R, \beta, T_\eta) = E_C(\beta, T_\eta) + V_P(\beta, T_\eta) + V_\ell(\beta, T_\eta). \quad (22)$$

The decay cross section is defined in terms of the partial waves as

$$\sigma = \frac{\pi}{k^2}\sum_{\ell=0}^{\ell_{\max}}(2\ell+1)P_0 P, \quad k = \sqrt{\frac{2\mu E_{\rm c.m.}}{\hbar^2}}. \quad (23)$$

Here $\ell_{\max}$ is the critical ℓ value (for the present work, its value is taken to be the same as in [18]).

III. RESULTS AND DISCUSSION

The complete charge minimized binary fragmentation potential of ^{181}Re* corresponding to one of the incident energies ($E_{\rm lab} = 77.18$ MeV) for two different angular momentum values ($\ell = 0$ and $40\hbar$) are shown in Fig. 1(a) as a function of the fragment mass number A_2. The fragmentation potential is evaluated assuming spherical fragments and interaction terms are treated as a function of T_η. The angular momentum has not changed the minimum present in the potential energy landscape. The potential energy is scaled as the angular momentum value increases. In this figure, the temperature for each channel is evaluated by fine-tuning the sharing of excitation energy between the fragments at the saddle (or a fixed ΔR value) corresponding to the incident energy of 77.18 MeV. The tuned temperature T_η is found to exhibit a strong structural variation, with prominent maximum values for the fragment pairs $A_2 = 44$, 46, 50, and 83 and their complementary values $A_1 = 137$, 135, 131, and 98 respectively. The fragment pairs corresponding to these maximum values are found to have minimum potential energy, as presented in Fig. 1(a). Within the fragmentation theory, a stronger minimum in the potential energy landscape indicates the most probable exit channel pairs of the fragments. These probable exit channel fragments are evident from the calculations of the preformation probability shown in Fig. 1(b) as a function of fragment mass numbers A_2 and A_1, corresponding to the potential energies presented in Fig. 1(a). The angular momentum scales the probability values, except for light fragments where no change in the probability values is seen as the angular momentum increases. Two prominent peaks are seen in the preformation probability values. However, considering the full mass window, the preformation probability values are found to be very low, and with an increase in angular momentum the change in probability is found to be only 3 to 5 orders of magnitude. Even at higher angular momentum values, the probability of preformation of the fission fragments of interest around $A = 75$ up to $A = 106$ is found to be very low.

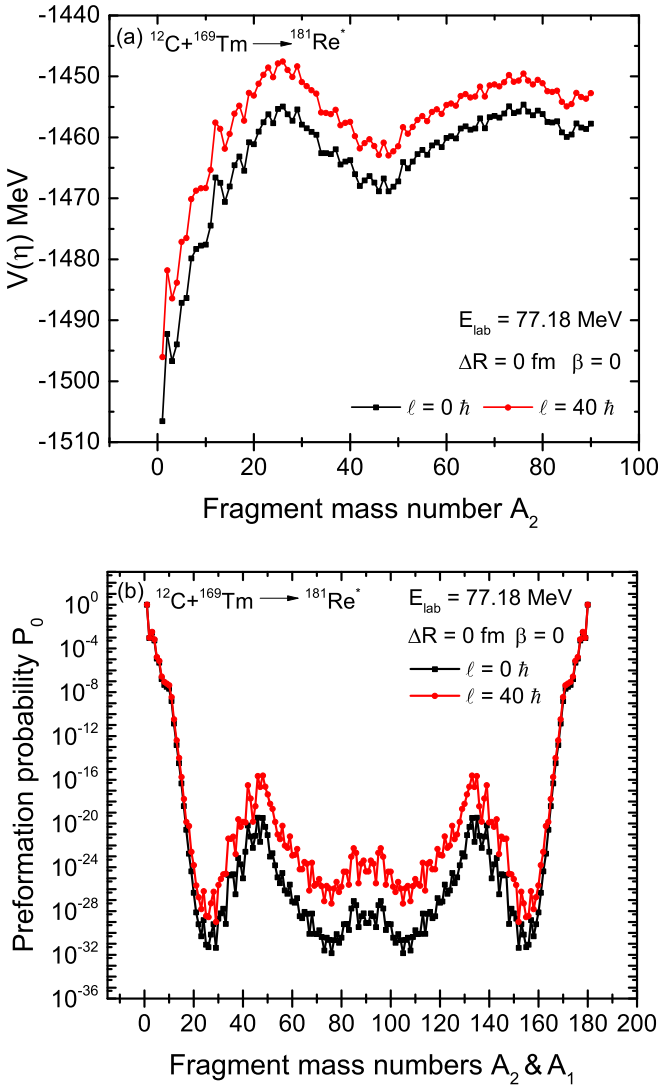

FIG. 1. (a) Fragmentation potential for the binary breakup of CN ^{181}Re* at $E_{\rm lab} = 77.18$ MeV using T_η for two different ℓ values corresponding to the ΔR value of 0 fm. (b) The preformation probability of all mass asymmetries corresponding to the potential energy of (a) assuming spherical fragments.

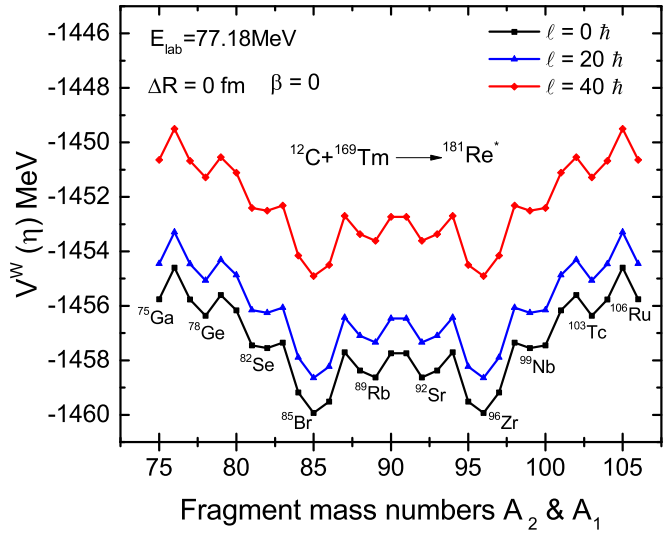

FIG. 2. The charge minimized fragmentation potential for the restricted mass range for the binary breakup of CN ^{181}Re* at $E_{\rm lab} = 77.18$ MeV using T_η for different ℓ values, assuming spherical fragments.

The experimental data of the fission fragments cross section are measured for a certain mass range, hence it becomes necessary to choose a convenient mass window for the present study, to see its role in the cross section values. Initially, we consider a mass range from 75 to 106, similar to that of experimental data. In Fig. 2, the plot of fragmentation potential energy for the mass window restricted case is shown. The superscript W denotes the window restricted mass range. This potential energy is the same as that presented in Fig. 1(a) but for the chosen mass window corresponding to different angular momentum values and for the use of the tuned channel temperature at $E_{\rm lab} = 77.18$ MeV. A closer observation indicates a three-nucleon transfer leading to the minima in the potential energies, with the deepest minimum occurring for the pair of fragments ^{85}Br and ^{96}Zr, with ^{85}Br having a neutron closed shell of $N = 50$. The structural variation present in potential energy is simply not an odd-even effect. We mention here that for very light mass nuclei, such as ^{56}Ni* formed in low energy heavy-ion collisions, the potential energy exhibits four-nucleon transfer, indicating preference of α-nuclei clusters such as ^{12}C, ^{16}O, etc. [8].

In order to understand the role of mass windows, in Figs. 3(a) and 3(b) the cross section distributions of various mass windows are presented for two different ΔR values corresponding to $E_{\rm lab} = 77.18$ MeV, assuming the fragments to be deformed. The solid line in both cases (a) and (b) corresponds to the cross section variation for the complete binary fragmentation from $A_2 = 1$. The distribution is slightly enhanced when the mass window is considered from $A_2 = 5$, indicating the influence of considering light particle emission on the same footing as that of heavy fragments. This result reveals that light particle emission and fission fragment emission have to be accounted for separately. With further restriction of the mass window (say $A_2 = 11$, 21, 31, 41, 51, 61, and 71), the variations of cross section values are found to be more or less comparable near the symmetric region. Hence, window restriction only influences the magnitude of cross section of fragments, with the most probable fragments remaining the same. At the same time, It is evident that the magnitude of cross section greatly changes with ΔR value, as shown in Fig. 3(b) for $\Delta R = 0.8$ fm.

In Figs. 4(a) and 4(b), the cross section distribution of the fission fragments corresponding to $E_{\rm lab} = 77.18$ MeV for two sets of different ΔR values are presented. The former plot shows the cross section values assuming fragments to be spherical and the latter gives a similar distribution considering deformed fragments. The calculations are carried out for the angular momentum $\ell_{\rm max}$ of $37\hbar$, as reported in the experiments corresponding to an incident energy of $E_{\rm lab} = 77.18$ MeV. The theoretical calculation of $\ell_{\rm max}$ in terms of the bombarding energy $E_{\rm c.m.}$ of the entrance channel is nearly

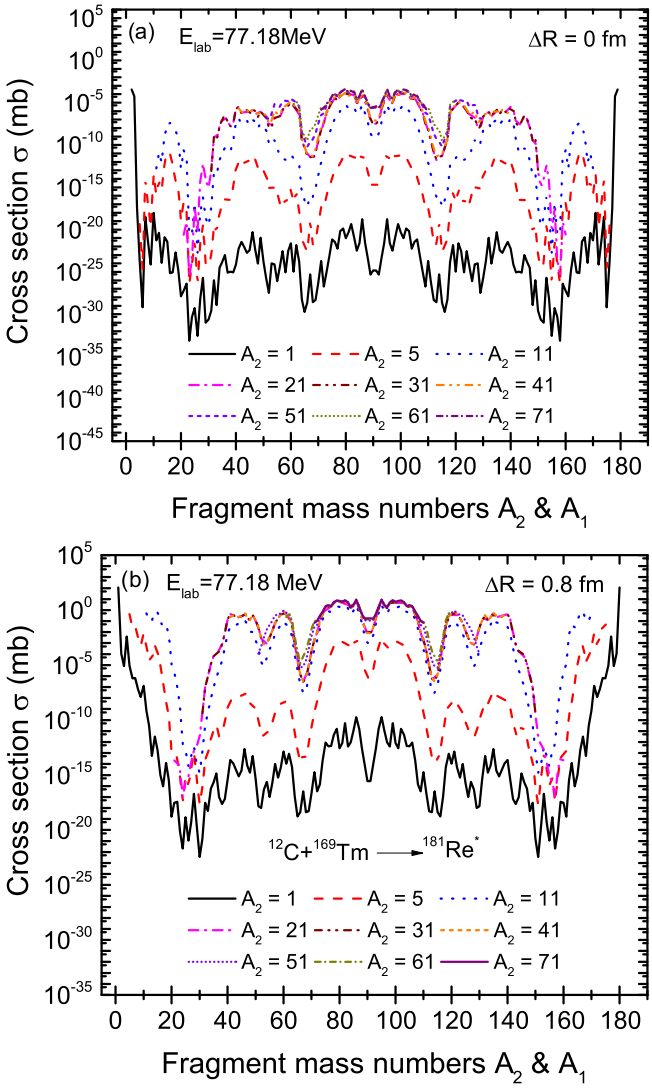

FIG. 3. The cross section variation for various mass windows including quadrupole deformation of fragments with neck length parameters (a) $\Delta R = 0$ fm and (b) $\Delta R = 0.8$ fm, corresponding to $E_{\rm lab} = 77.18$ MeV.

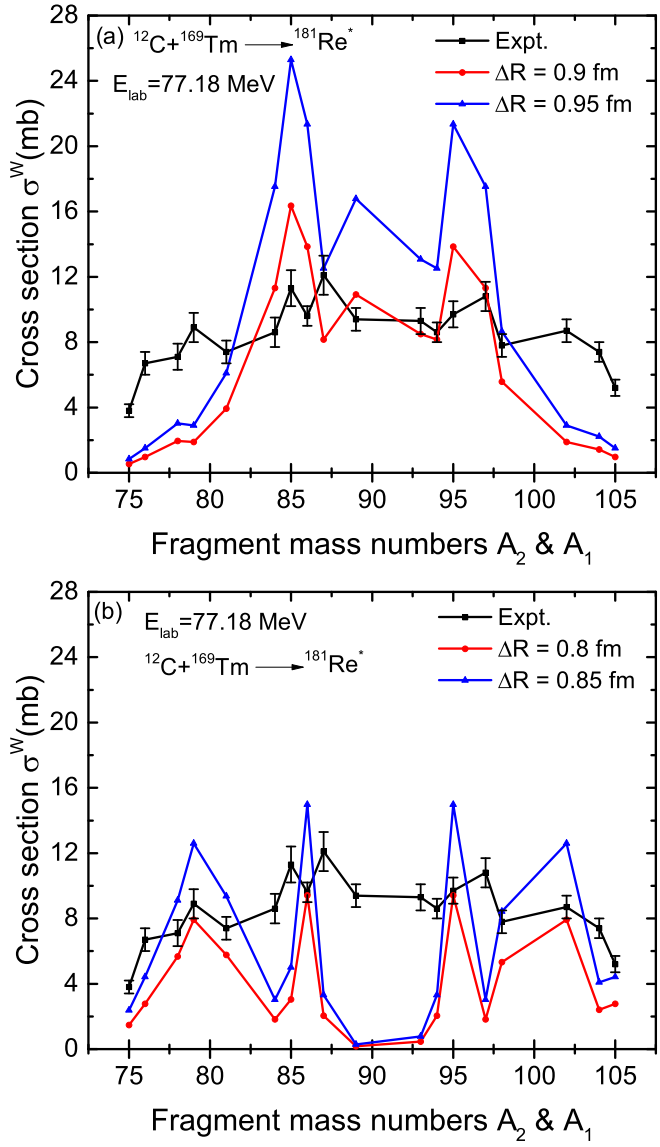

FIG. 4. (a) The cross section distribution of spherical fission fragments for the restricted mass window for $E_{\rm lab} = 77.18$ MeV, taking two ΔR values 0.9 fm and 0.95 fm. (b) Similar to (a), but for the deformed fission fragments with ΔR of 0.8 and 0.85 fm.

equivalent to the experimental observation for the three incident energies, and it is seen that the cross section distribution does not change much with $\ell_{\rm max}$. For the other two incident energies of 83.22 and 89.25 MeV, the $\ell_{\rm max}$ values are taken as $41\hbar$ and $45\hbar$ respectively. The role of the neck length parameter has much influence on the outcome. The comparison with experimental data for the three energies considered clearly indicates the importance of inclusion of deformation in the model, because the spherical calculation exhibits a two humped distribution whereas the deformed calculation exhibits strong structural variation like the experimental data. Further, the importance of neck distance ΔR is evident. We mention that, in the present study, fine-tuning of the parameter ΔR for each channel is not done; rather a bound of two ΔR values is given, within which the model would fairly compare with experimental data. The poor comparison for the fragment pairs around the symmetric region may be due to the fact that,these fragments are just away from the neutron closed shell of $N = 50$. A further analysis is needed, by considering higher order deformations in the model calculations. The obtained results indicate that the fine-tuning of the parameter ΔR may give a better comparison. The role of ΔR is similar to that of fixed deformation β for all the fragments. The cross section obtained with fixed β for all fragments shows a distribution similar to that of the result with a definite ΔR.

For the other two $E_{\rm lab}$ energies similar results are obtained, and are presented in Fig. 5. The calculated values correspond to deformed fragments with ΔR values of 0.8 and 0.85 fm. The solid line with squares shows the experimental cross section along with the experimental uncertainty. The solid lines with triangles and circles correspond to the cross section

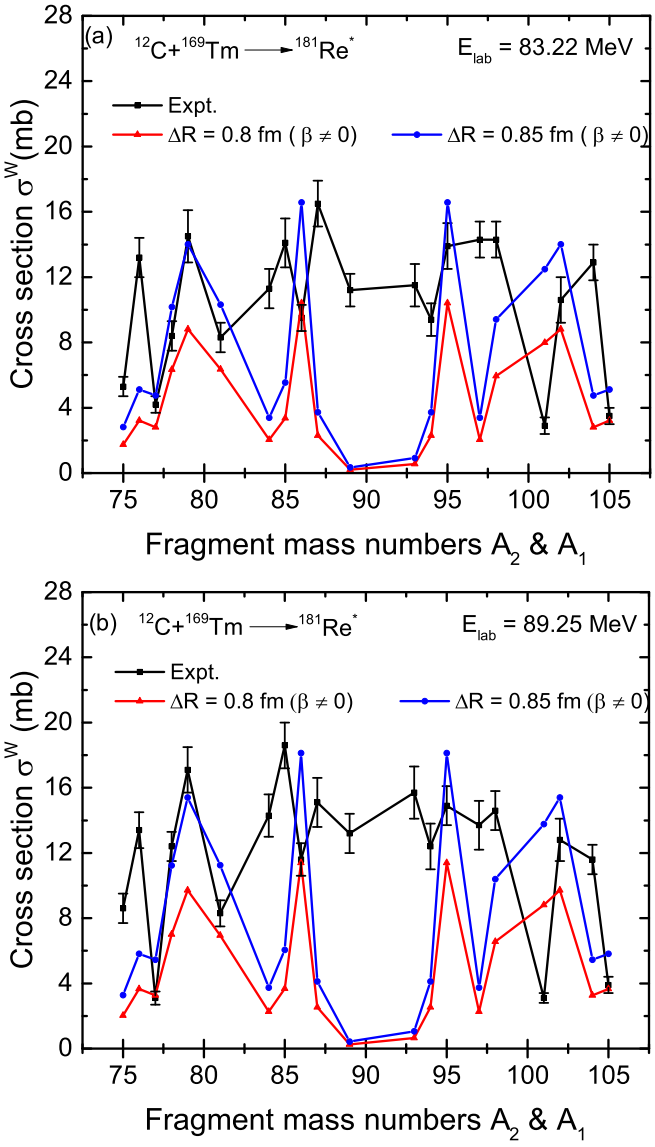

FIG. 5. (a) The cross section variation for the decay of ^{181}Re* corresponding to $E_{lab} = 83.22$ MeV for deformed fragments ($\Delta R =$ 0.8 and 0.85 fm). (b) Similar to (a), but for $E_{lab} = 89.25$ MeV.

obtained by treating fragments as deformed for ΔR of 0.8 and 0.85 fm respectively. Overall, our model results are found to fairly compare with the experimental data.

IV. SUMMARY

The dynamical cluster-decay model developed for the decay of hot and rotating compound nuclei is applied to study the binary decay of ^{181}Re* formed through the reaction $^{12}C + ^{169}Tm$ for three different experimentally reported incident energies. In DCM, we have incorporated the aspects of channel temperature and mass window restriction for spherical and deformed fragments. By conserving the sum of excitation energies of individual fragments and the excitation energy of the compound nucleus at saddle distance, the fragment temperature for a given channel (mass asymmetry) is evaluated. Further, as the experimental data are available for a certain mass range, we have considered the mass window range from $A = 75$ to 106 in the model. The window restricted DCM picture with channel temperature is used to calculate the preformation (P_0) probability within the fragmentation theory. Combining preformation probability P_0 with penetration probability P, the fission decay cross section is evaluated for three E_{lab} energies: 77.18, 83.22, and 89.25 MeV, with neck-length parameter $\Delta R = 0.9$ fm for spherical fragments and $\Delta R = 0.8$ fm for deformed fragments. The comparison of the cross section with the experimental result indicates a dependence on ΔR, T_η, and deformation of fragments in the evaluation of fission observables. The window restriction does not influence the cross section distribution of fission fragments when binary fragmentation is considered above $A_2 = 11$. For better comparison with the experimental data, window restriction is needed, as indicated by the results of the preformation probability and cross section calculations. With full window consideration, the probability of fission fragments of interest is found to have very low values. However, with the restriction of the mass window, an enhanced probability can be obtained for the experimentally observed fission fragment mass range. The other aspect considered, namely, the channel temperature, exhibits structural variation in the cross section values near the symmetric breakup. A better comparison may be obtained by fine-tuning the free parameter of the model, which is not attempted.

ACKNOWLEDGMENT

C.K. acknowledges financial support in the form of a DST-INSPIRE Research Fellowship, vide sanction No. DST/INSPIRE FELLOWSHIP/[IF170021] awarded by Department of Science and Technology, Government of India.

[1] T. Matsuse, C. Beck, R. Nouicer, and D. Mahboub, Phys. Rev. C **55**, 1380 (1997).
[2] S. J. Sanders, Phys. Rev. C **44**, 2676 (1991).
[3] S. Sanders, A. de Toledo, and C. Beck, Phys. Rep. **311**, 487 (1999).
[4] B. Wilkins and E. Steinberg, Phys. Lett. B **42**, 141 (1972).
[5] J. F. Lemaître, S. Panebianco, J.-L. Sida, S. Hilaire, and S. Heinrich, Phys. Rev. C **92**, 034617 (2015).
[6] R. K. Gupta, M. Balasubramaniam, C. Mazzocchi, M. La Commara, and W. Scheid, Phys. Rev. C **65**, 024601 (2002).
[7] M. Balasubramaniam, R. Kumar, R. K. Gupta, C. Beck, and W. Scheid, J. Phys. G: Nucl. Part. Phys. **29**, 2703 (2003).
[8] R. K. Gupta, R. Kumar, N. K. Dhiman, M. Balasubramaniam, W. Scheid, and C. Beck, Phys. Rev. C **68**, 014610 (2003).
[9] R. K. Gupta, M. Balasubramaniam, R. Kumar, D. Singh, and C. Beck, Nucl. Phys. A **738**, 479 (2004).
[10] R. K. Gupta, M. Balasubramaniam, R. Kumar, D. Singh, C. Beck, and W. Greiner, Phys. Rev. C **71**, 014601 (2005).

[11] R. K. Gupta, M. Balasubramaniam, R. Kumar, D. Singh, S. K. Arun, and W. Greiner, J. Phys. G: Nucl. Part. Phys. **32**, 345 (2006).
[12] B. B. Singh, M. K. Sharma, and R. K. Gupta, Phys. Rev. C **77**, 054613 (2008).
[13] C. Karthikraj, N. S. Rajeswari, and M. Balasubramaniam, Phys. Rev. C **86**, 014613 (2012).
[14] H. J. Krappe, Phys. Rev. C **59**, 2640 (1999).
[15] C. Kokila and M. Balasubramaniam, Phys. Rev. C **100**, 034607 (2019).
[16] M. T. Senthil Kannan and M. Balasubramaniam, Eur. Phys. J. A **53**, 164 (2017).
[17] C. Karthika and M. Balasubramaniam, Eur. Phys. J. A **55**, 59 (2019).
[18] A. Sood, P. P. Singh, R. N. Sahoo, P. Kumar, A. Yadav, V. R. Sharma, M. Shuaib, M. K. Sharma, D. P. Singh, U. Gupta, R. Kumar, S. Aydin, B. P. Singh, H. J. Wollersheim, and R. Prasad, Phys. Rev. C **96**, 014620 (2017).
[19] M. Maiti, J. Radioanal. Nucl. Chem. **290**, 11 (2011).
[20] S. Lahiri, K. Mukhopadhyay, K. Banerjee, A. Ramaswami, and S. Manohar, Appl. Radiat. Isotopes **55**, 751 (2001).
[21] S. Chakrabarty, B. Tomar, A. Goswami, G. Gubbi, S. Manohar, A. Sharma, B. Bindukumar, and S. Mukherjee, Nucl. Phys. A **678**, 355 (2000).
[22] A. Sharma, B. B. Kumar, S. Mukherjee, S. Chakrabarty, B. S. Tomar, A. Goswami, G. K. Gubbi, S. B. Manohar, A. K. Sinha, and S. K. Datta, Pramana **54**, 355 (2000).
[23] M. K. Sharma, P. P. Singh, D. P. Singh, A. Yadav, V. R. Sharma, I. Bala, R. Kumar, Unnati, B. P. Singh, and R. Prasad, Phys. Rev. C **91**, 014603 (2015).
[24] A. Gavron, Phys. Rev. C **21**, 230 (1980).
[25] R. K. Gupta, W. Scheid, and W. Greiner, J. Phys. G: Nucl. Part. Phys. **17**, 1731 (1991).
[26] W. Greiner and R. K. Gupta, *Heavy Elements and Related New Phenomena* (World Scientific, Singapore, 1999), https://www.worldscientific.com/doi/pdf/10.1142/3664
[27] J. Maruhn and W. Greiner, Phys. Rev. Lett. **32**, 548 (1974).
[28] R. K. Gupta, W. Scheid, and W. Greiner, Phys. Rev. Lett. **35**, 353 (1975).
[29] J. Maruhn and W. Greiner, Z. Phys. **251**, 431 (1972).
[30] P. Moller, J. Nix, W. Myers, and W. Swiatecki, At. Data Nucl. Data Tables **59**, 185 (1995).
[31] W. D. Myers and W. J. Swiatecki, Nucl. Phys. **81**, 1 (1966).
[32] V. Y. Denisov and N. A. Pilipenko, Phys. Rev. C **76**, 014602 (2007).
[33] V. Y. Denisov, N. A. Pilipenko, and I. Y. Sedykh, Phys. Rev. C **95**, 014605 (2017).
[34] J. Blocki, J. Randrup, W. Swiatecki, and C. Tsang, Ann. Phys. (NY) **105**, 427 (1977).
[35] H. Kroger and W. Scheid, J. Phys. G: Nucl. Phys. **6**, L85 (1980).